

Decentralized reinforce-control of renewable dynamic virtual power plant enabling it to offer ancillary services: An attempt towards net-zero targets

Lalit Kumar¹  | Shehab Ahmed¹ | Raj Naidoo² | Ramesh Chand Bansal^{2,3}

¹Computer, Electrical and Mathematical Science and Engineering Division (CEMSE), King Abdullah University of Science and Technology (KAUST), Saudi Arabia

²Department of Electrical, Electronic and Computer Engineering (EECE), University of Pretoria, Pretoria, South Africa

³Department of Electrical Engineering, University of Sharjah, Sharjah, United Arab Emirates

Correspondence

Lalit Kumar, Computer, Electrical and Mathematical Sciences and Engineering, KAUST, Thuwal, Saudi Arabia.

Email: lalitnbd@gmail.com

Funding information

King Abdullah University of Science and Technology (KAUST), Saudi Arabia, Grant/Award Number: OSR-2019-CoE-NEOM-4178.12; Department of Library Services, University of Pretoria, South Africa

Abstract

This article presents internal model control (IMC) based decentralized reinforce-control of renewable dynamic virtual power plant (DVPP) so that, it can be integrated into the power system as a substitution of fuel-based conventional generators. Such grid integration towards net-zero targets could not be possible without providing additional ancillary service (AS) to the power system, as the traditional AS would fall short with the retirement/substitution of conventional generators. The theory of DVPP from a technical perspective (i.e., TDVPP) is presented in a detailed and simplified manner, including the formulation of a generalized control objective (desired specification) for DVPP integration. The solution approach includes two steps: (1) disaggregation of desired specification and (2) decentralized reinforce-control to match the disaggregated specification. The theory and solution approach for DVPP integration is presented in a generalized manner enabling the DVPP to offer multiple ASs, but the case study is limited only to frequency control AS (FCAS) in this article. The study is performed on the 'western system coordinating council (WSCC)' test system, in which an attempt is made towards net-zero targets by substituting the largest thermal generator with renewable DVPP ensuring the grid's operation or dynamics safe.

1 | INTRODUCTION

Stability is a major concern for reliable power system operation. The stability of a power system is the ability to return to an equilibrium state progressively, after being subjected to contingency events such as short-circuit, line or generator tripping etc. [1]. The stability is ensured by maintaining the frequency and voltage magnitudes in the entire power system networks within safe acceptable limits, with the help of several regulations and control schemes. The stability is ensured by maintaining the frequency and voltage magnitudes in the entire power system networks within safe acceptable limits with the help of several regulations and control schemes. One of the conducive factors to stability is the inherent large rotational inertia of the synchronous generator (SG), as it is a first response to the system after a frequency excursion event [2]. Though inertial response (IR) does not balance the supply and demand, it lim-

its the initial rate at which the frequency falls buying some time for other control services to act [3]. The increasing integration of renewable energy sources (RESs) and the retirement of SG-based power plants have resulted in a significant reduction in equivalent inertia of the power systems incurring critical stability challenges [4–6]. Contingency events in such low-inertia power systems can trigger frequency protective relays leading to a cascade failure [7, 8]. Few performance metrics that are used to quantify low-inertia power systems are frequency nadir, rate of change of frequency (RoCoF), arresting period, and power system damping ratio [2, 5, 7].

The RESs being integrated for net-zero targets should also play a role in providing ancillary services (ASs) to support the grid, or at least not to harm the grid [9]. The arrival of the COVID-19 virus has further triggered the need for ASs in the following two ways: (1) In low net demand during the lockdown, the carbon-based plant was planned to be shut off.

This is an open access article under the terms of the [Creative Commons Attribution-NonCommercial-NoDerivs](https://creativecommons.org/licenses/by-nc-nd/4.0/) License, which permits use and distribution in any medium, provided the original work is properly cited, the use is non-commercial and no modifications or adaptations are made.

© 2022 The Authors. *IET Renewable Power Generation* published by John Wiley & Sons Ltd on behalf of The Institution of Engineering and Technology.

As a result, the share of carbon-free generation was expected to be increased, resulting in a need for additional ASs for the healthy operation of the grid. (2) The low net demand in lockdown had allowed the power system to have a temporary outage of various network parts, for example, plant, line other equipment etc., providing the right occasion to do any modifications at a mass scale such as installation of ASs. Learning from the China and European nation's lockdown, Great Britain's power system conducted a study in March 2020 and projected the reduction in net demand if a lockdown is put in place [10]. As a result, the quantity and types of ASs to be required during the lockdown were reviewed [10]. The scope and significance of AS-related study further increased, as the new COVID-19 variants continue to emerge, resulting in the nations undergoing partial/full lockdown again.

RESs alone are incapable to provide such services due to their fluctuating outputs and energy (or power) limitations, however, RESs in conjunction with energy storage systems (ESSs) as a whole can help reduce the unwanted frequency/voltage deviations much faster than conventional generation [7, 8] and as a result, the idea of a virtual power plant (VPP) has evolved. VPP is a collection of heterogeneous RESs and/or ESSs, which may present itself to the grid as a single dispatchable and controllable virtual SG [11, 12]. ESSs as a constituent of VPP can compensate (internally balance) the fluctuating generation by constituent RESs [13]. VPP is generally classified into two categories: commercial VPP (CVPP) and (2) technical VPP (TVPP) [12]. CVPP aims at an economic profit and TVPP aims not only on the safe operation of VPP but the safe operation of the grid as well by providing AS [11, 12]. Further ahead, the new paradigms were defined to make VPP a dynamic VPP (DVPP) [14, 15]. The main feature of DVPP is envisioned as the ability of it to act as a synchronous VPP (SVPP) that could emulate the characteristics of conventional synchronous generators [16].

DVPP has been studied mostly in perspective to CDVPP [11, 17] but recently, the authors [16] have studied it in perspective to TDVPP wherein the DVPP was referred to SVPP. The authors have upgraded the VPP to DVPP by placing adjustable inertia support at the converters which is controlled by an online learning-based method. The approach involved complex 'multivariable centralized control', wherein the units of DVPP were controlled according to the individual's desired specification and not according to the global desired specification. In other words, DVPP as a whole has not been made accountable to meet the desired specification. In [18, 19], the authors presented a comprehensive review on grid integration of renewables and, it is reported that ESSs are a viable and economical solution to achieve the ASs by grid integration. In [20], a rare practical study is presented with the integration of large-scale battery ESSs (BESSs) at the distribution level in an Indian power grid. Two different battery packs, that is, lithium-ion and advanced lead-acid, with a total capacity of 1 MW were integrated at a 22kV medium distribution system. The important findings were: (1) the maximum utilization of BESSs was attained while operating it for frequency regulation or FCAS (2) the BESS being operated for FCAS, significantly improves the voltage profile as well (3) it is desirable to use the mixed battery packs to best achieve the economical and technical targets [20].

Most of the related study in the past calls for modifications in the in-built control of converters [16]. In this article, the DVPP is controlled to provide the desired ASs/specifications in such a way that, the already deployed converters at the mass scale needs not be touched from the inside of its cabinet. Only the reference port of the converter corresponding to desired AS is needed for the placement of the proposed reinforce-control which is then decentralized at the DVPP level and not at the centralized level.

This article presents the study with renewable DVPP from its technical perspective (i.e., TDVPP) which is controlled to offer AS to make its integration sustainable and safe for the grid. The control objective, that is, desired specification is disaggregated in proportion to 'participation factors (PFs)' among the units of DVPP. Then, internal model control (IMC) based decentralized reinforce-control is implemented to achieve/match the disaggregated specification. Being the most important AS, only frequency control AS (FCAS) is focused on in this article. The main contributions are as follows;

- (i) Review-based classification of ASs, being discussed in a confined manner
- (ii) Theorization and formulization of the control problem for the DVPP for its sustainable grid integration.
- (iii) Invention and the adoption of PFs to disaggregate the desired DVPP's specification.
- (iv) Development and implementation of IMC-based decentralized reinforce-control to match the disaggregated specification.

Apart from grid integration, ASs, and DVPP, the study here covers one more research topic, that is, nonminimum phase behaviour (NPB) of hydro plant [21], which is resolved as a by-product of the solution approach, adopted for DVPP integration.

The rest of the article is organized as follows: Section 2 presents the rigorous review of the ASs. Section 3 theorizes the DVPP from a technical perspective to offer ASs. Section 4 presents the solution approach for DVPP in the form of decentralized reinforce-control inventing and adopting the PF. Section 5 presents a brief discussion on general assumptions, causality issues, and choice of PFs, in regards to the solution approach. Section 6 familiarises the test system and DVPP to be integrated into the test system. Section 7 presents the case studies on DVPP integration into the test system. Lastly, conclusions are drawn in Section 8.

2 | REVIEW ON ASs

The adverse impact of RESs integration on basic 'system services' such as generation, transmission, and distribution has led to the emergence of ASs [22]. System services are provided by the system operator to all users in the network, whereas, ASs are provided by some of the users (prosumers) to the network on the behest/procurement by the system operator [23]. The purpose of AS is not only to conduce the system service under contingency events but to conduce all stability aspects of wide range grid operation [1, 22]. Traditionally, ASs are provided by

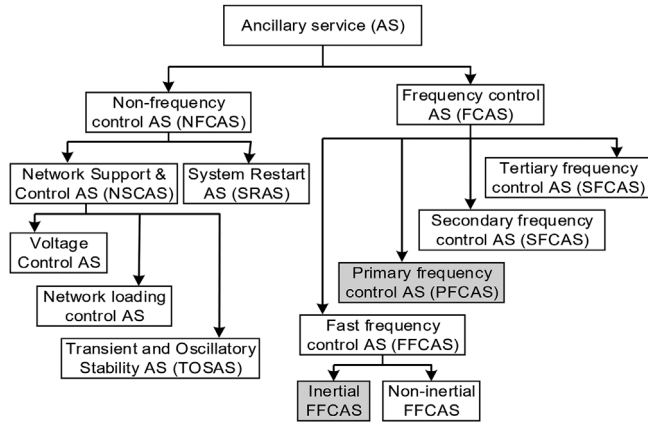


FIGURE 1 Classification of ancillary service (AS)

large-scale power plants, storage resources (e.g., capacitors or pumped hydro storage), and reactive power control equipment (e.g., capacitor banks or static compensators) with sufficient capacity and capability [22, 24], which are no longer sufficient, as the variable RESs' integration continues to grow [22, 24]. The paradigms of new ASs are being defined and classified at various levels especially considering the fast-acting capability of converter interfaced units (CIUs), that is, converter interfaced RESs or ESSs [8, 22, 25, 26]. Apart from CIUs, HVDC converters also have been seen as a great medium to provide ASs [27, 28] on a large-scale.

It was found that there is no standardized classification of ASs. These are classified by the transmission system operator (TSO) based on the individual power systems and their regional requirements [22, 23, 25]. FCAS is reported to be the most renowned and important AS in the literature as well as in the industrial reports [1, 8], therefore the ASs in this article have been classified into two categories: Non-frequency control AS (NFCAS) and FCAS [24, 29]. The detailed classification is charted in Figure 1 which is discussed next, however, only FCAS will be discussed in detail, being the interest in this article.

2.1 | Non-FCAS

2.1.1 | Network support and control ASs (NSCASs)

As shown in Figure 1, there exist three categories of NSCASs;

- (i) **Voltage control ASs:** These ASs control the voltage at various points in the power system network to maintain it within the prescribed limits. The basic voltage control ASs are provided from generators through automatic voltage regulators (AVRs), while enhanced voltage control ASs are generally been provided from the synchronous condenser, static reactive plant (capacitors/reactors) [7, 23]. CIUs are the recent contributors to these ASs [29].

- (ii) **Network loading control ASs:** These ASs are used to control the line flow to maintain it within the prescribed limits through increasing/decreasing generation or by load shedding [26].
- (iii) **Transient and oscillatory stability ASs:** These ASs fast-regulate and control voltage/power injection in the network, or speedily decrease/increase the connected loads. Some examples are: power system stabilizers (PSS), and fast regulating services (synchronous condensers, SVCs etc.) [26]. CIUs are the recent contributors to these ASs [19].

2.1.2 | System restart ASs (SRAS)

System restart ASs or black start capability are required to restart the power system following a complete or partial blackout. Hydropower plants (pump-storage and run-of-river) are known to be very efficient in providing SRAS [30]. Thermal, compressed gas plants, and diesel generators are a few other options for such services [30].

2.2 | FCAS

These are ASs used to maintain frequency within the prescribed limit by balancing load and generation in real-time. In a traditional power system, there were mainly three levels of control to achieve FCAS, that is, (1) primary frequency control AS (PFCAS) (2) secondary frequency control AS (SFCAS) (3) tertiary frequency control AS (TFCAS). These controls are generally characterized and distinguished by their application time range.

2.2.1 | PFCAS

The PFCAS mainly helps in containing the frequency nadir/zenith and stabilizing it at a new steady-state value, leaving its restoration to SFCAS [31, 32]. Therefore, the reserve to provide this AS is generally called frequency containment reserve (FCR). Turbine governor (TG) control or load frequency control is a traditional method to provide this service [7, 33], in which the response is proportional to the frequency deviation [5]. CIUs are the recent contributors to these ASs [13]. The typical application time range for PFCAS is 10–30 s after the start of the frequency excursion event [1, 7].

2.2.2 | SFCAS

These ASs are provided by 'automatic frequency restoration reserves' (aFRRs) through automatic generation control (AGC) of the region [33]. The target is to restore the nominal frequency and the primary reserve capacity as well [7, 24]. SFCAS gradually replaces the PFCAS after 30 s and activates fully within 5 minutes of frequency excursion instant, and lasts up to 15 minutes [24].

2.2.3 | TFCAS

These ASs are provided by ‘manual frequency restoration reserves’ (mFRRs) in further need of frequency regulation or when regional congestion and imbalances are to be handled in the grid. These are manual reserves that gradually substitute SFCAS and activate fully within 15 minutes of frequency excursion instant [1, 24].

As discussed before, the low-inertia power system is no longer able to arrest the initial frequency variations (RoCoF, nadir/zenith) before the PFCAS could activate. Traditional PFCAS cannot respond within that little time range (<10 s) [7], which leads to a drop/rise in frequency beyond the acceptable limits in the first few cycles. Therefore, a new category of FCAS has evolved known as fast frequency control AS (FFCAS), which is undergirded by the fast responding capability of CIUs.

2.2.4 | FFCAS

These are the ASs that provides a quick response to the frequency variations in the form of controlled electrical power contribution to the grid during the arresting phase of a frequency excursion event such that the subdued IR is compensated [8, 9, 34].

Some authors do not discriminate FFCAS from PFCAS and consider it as a fast PFC [4, 7, 8]. However, the majority of authors put FFCAS in a separate category then PFCAS [9], mainly because FFCAS is provided through the controlled electrical power (fast) from various sources/storages (CIUs), whereas PFCAS is traditionally provided through the controlled mechanical power (slow) of SGs [9]. FFCAS is a short-term response service with relatively less energy reserve than PFCAS [13, 24, 33], which is supposed to activate within 1 s of the frequency excursion instant [7, 8]. If placed with sufficient reserve, the involved CIUs in FFCAS can also continue to provide PFCAS as well [8, 13].

FFCASs are reported to have ambiguity in their performance objectives, technical specifications, and functional orientation. The main ambiguity remained in addressing it as an inertia emulation service [9]. Many authors have clarified that the inertia emulation services, that is, virtual-inertia or synthetic-inertia are a subset of FFCAS [7, 9, 34], which will be clarified further here, but before that, it is necessary to understand the inertia dynamics first.

Inertia is an inherent characteristic of SG defined as the ability to discharge or store kinetic energy subjected to the sudden power imbalance, without undergoing rotational speed variations [8, 21, 32, 34]. The stored kinetic energy in the spinning masses presents itself as a reserve for FFCAS, which relates to the inertia constant by the following equation in the mechanical domain [3, 31].

$$K.E = \frac{1}{2} J \omega^2 = H \cdot S_N, \quad (1)$$

where H is the inertia constant in a second, J is the moment of inertia in kg.m², ω is the angular velocity and S_N is the

nominal apparent power of the SG. Further, the electro-mechanical dynamic of SGs involving the inertia constant is governed by the swing equation as follows [5, 35];

$$\frac{2H}{f_n} \frac{df}{dt} = p_m - p_e = \Delta p, \quad (2)$$

where f is the frequency in Hz and f_n is its nominal frequency, p_m and p_e are the mechanical turbine power and electrical power in p.u., respectively, Δp is the generation load imbalance. Similar dynamics can be achieved for the equivalent power system model by adding all such involved dynamics. The total load generation imbalance can be obtained as follows [35];

$$\Delta P = \sum_{i=1}^N \Delta p_i = \frac{2 \sum_{i=1}^N H_i}{f_n} \frac{df_c}{dt} = \zeta \frac{df_c}{dt}, \quad (3)$$

where

$$f_c = \frac{\sum_{i=1}^N H_i f_i}{\sum_{i=1}^N H_i} \quad \& \quad \zeta = \frac{2}{f_n} \sum_{i=1}^N H_i, \quad (4)$$

are the centre of inertia (COI) frequency and a constant, respectively [35]. Equation (3) indicates that the instantaneous RoCoF ($\frac{df_c}{dt}$) is depending on two factors: (1) inertia constants and (2) the net power imbalance (size of the event) [31, 32]. Indeed, the impact of low inertia caused the existence of FFCAS, but emulating the inertia is not the only way to reduce the impact. The impact can be reduced by minimizing the power imbalance by other means as well [36]. So, FFCAS can further be categorized into two categories: (1) inertial FFCAS (2) non-inertial FFCAS.

- (i) **Inertial-FFCAS:** Following the typical inertia dynamics of SGs (Equation 2), the virtual inertia can be emulated by the CIUs, if provided with the short-term fast energy reserve, analogous to SG’s kinetic energy reserve [2, 33, 34] and thus the associated inertial services are referred as inertial FFCAS. These services are provided locally at the generating units by instantly injecting the controlled additional power (from reserve) proportional to the RoCoF sensed at PCC [31, 34, 36].
- (ii) **Non-inertial FFCAS:** Any other form of FFCAS excluding inertial FFCAS which helps in counteracting the impact of low-inertia, can be referred to as non-inertial FFCAS. Unlike inertial FFCAS, controlled electrical power contribution is not proportional to RoCoF in non-inertial FFCAS, and not necessarily be injected at the PCC of generating unit. The following may be some non-inertial FFCAS [7, 9]: (a) Active power injection (-ve or +ve) in proportion to measured frequency deviation (Δf) (b) Constant active power injection based on the detection of frequency deviation threshold (Δf_{thres}) or RoCoF threshold ($\frac{df}{dt}_{thres}$) (c)

Controlled load reduction in proportion to Δf or RoCoF
 (d) Controlled reduction of constant load based on the
 detection of Δf_{thres} or $\frac{df}{dt}_{thres}$.

Among the discussed categories of ASs above, the worst impact of low IR has been reported on PFCAS and FFCAS (PFCAS+FFCAS) [5, 9, 13], and ESSs have been proven to be the best solution for both [13]. Also, FFCAS from one location taken over by PFCAS at a different location may excite inter-regional power oscillations [9]. Therefore, it is desirable to provide these both ASs from the same generating station. But, how much IR or primary frequency response (PFR) is to be emulated by a generating unit depends on real-time equivalent inertia estimation, which is still in its infantile stage. One of the best practices for providing FCAS is to emulate the thermal SG behaviour from a generating station [6]. Next, we introduce the technical perspective of DVPP, which aims to provide PFCAS+FFCAS (inertial).

3 | THEORIZATION OF DVPP: TECHNICAL PERSPECTIVE

3.1 | General structure

From the technical perspective, DVPP can be assumed as advanced VPP with advanced control making it capable to provide the dynamic (fast) ASs. Heterogeneity among the units is a very important aspect in the formation of DVPP since none of the individual units alone is able to provide these services consistently across all power and energy levels (entire frequency domain). Some units may provide a fast response but have low energy density (short-term), whereas some may provide a slow response, but are rich in energy density (long-term). But, a sufficient number of heterogeneous ensemble units will be able to do so.

Depending on inputs/outputs, the control method for the DVPP can be divided into two categories: (1) multivariable centralized control and (2) common variable decentralized control, as depicted in Figure 2. The constituent units in DVPP are depicted by G_i . The figure is drawn considering the single input single output (SISO) system, just to show the differences in the control method. The depicted control structure for each unit is a generalized control structure with one controller in the feed-forward path and the second in the feedback path. The control structure and highlighted red text in Figure 2 are left for later discussions. The existing centralized control method (Figure 2a) is naive, not robust, and fails if individual modules of the DVPP fail. Moreover, it mostly involves optimization-based controllers which are complex, hard to implement, and typically not stable under interconnections. In this article, the common variable decentralized control method (Figure 2b) has been adopted, in which, the desired specification is disaggregated to individual units in the DVPP.

3.2 | DVPP theory

Consider a model of a i^{th} unit in a DVPP as follows;

$$S_i \begin{cases} \dot{x}_i = \mathcal{A}_i x_i + \mathfrak{B}_i u \\ y_i = C_i x_i + \mathfrak{D}_i u \end{cases} \quad \forall i \in [1 N], \quad (5)$$

where $\mathcal{A}_i \in \mathbb{R}_i^{n \times n}$, $\mathfrak{B}_i \in \mathbb{R}_i^{n \times I}$, $C_i \in \mathbb{R}_i^{O \times n}$ and $\mathfrak{D}_i \in \mathbb{R}_i^{O \times I}$ being the state matrix, input matrix, output matrix and feedforward matrix, respectively. The variables, $x_i \in \mathbb{R}_i^{n \times 1}$, $y_i \in \mathbb{R}_i^{O \times 1}$ and $u \in \mathbb{R}^{I \times 1}$ are the state, output, and input variables, respectively, and, the latter will be common to all units, S_i . The region, ' \mathbb{R} ' maps the dimension of the matrix and ' n ' represents the order of the unit model, S_i . The parameters, I & O in the superscript represents the number of inputs and outputs of S_i , respectively.

For all grid-following ASs, O can be fixed as $O = 2$, since ultimately, all the desired specifications have to be provided by injecting two aggregated outputs, that is, P and Q , through appropriate control. By conversion theory of the multi-input multi-output (MIMO) systems [37], any MIMO system of the form, S_i shown in Equation (5) can be converted into MIMO transfer function (TF) form as follows;

$$S_i \left\{ \begin{bmatrix} y_i^1 \\ y_i^2 \end{bmatrix} \right\} = \begin{bmatrix} G_i^{11} & \dots & G_i^{1I} \\ G_i^{21} & \dots & G_i^{2I} \end{bmatrix} \begin{bmatrix} u_1 \\ \vdots \\ u_I \end{bmatrix}, \quad (6)$$

$$\Rightarrow y_i = G_i \cdot u. \quad (7)$$

Here onwards, the study is presented in the 's' domain, however, '(s)' is avoided in writing for ease. For CIUs as well as SG, the outputs, y_i^1 , that is, P and y_i^2 , that is, Q can be controlled in a decoupled manner [38], thus the unit-model, S_i can be represented in segregated P-Q form (\tilde{S}_i) as follows;

$$\tilde{S}_i \left\{ \begin{bmatrix} y_i^1 \\ y_i^2 \end{bmatrix} \right\} = \begin{bmatrix} G_i^P & 0_{1 \times K} \\ 0_{1 \times J} & G_i^Q \end{bmatrix} \begin{bmatrix} u_P \\ u_Q \end{bmatrix}, \quad (8)$$

$$\Rightarrow y_i = \tilde{G}_i \cdot \tilde{u}, \quad (9)$$

where J & K in the subscript are the number of P-class inputs, u_P and Q-class inputs, u_Q , respectively. \mathbb{P}, \mathbb{Q} being the 'index selecting and grouping operators' for u_P and u_Q , that is,, $u_P = \mathbb{P}(u)$, $u_Q = \mathbb{Q}(u)$, $\ni u_P, u_Q \subseteq u$ and $G_i^P = \mathbb{P}(G_i)$, $G_i^Q = \mathbb{Q}(G_i)$, $\ni G_i^P, G_i^Q \subseteq G_i$.

3.3 | Formulation of the control problem

Summing/pooling all the outputs from the N number of uncontrolled units in DVPP defined by Equation (9), the aggregated output of the DVPP can be obtained as;

$$y_{agg} = \sum_{i=1}^N y_i = \left(\sum_{i=1}^N \tilde{G}_i \right) \cdot \tilde{u}. \quad (10)$$

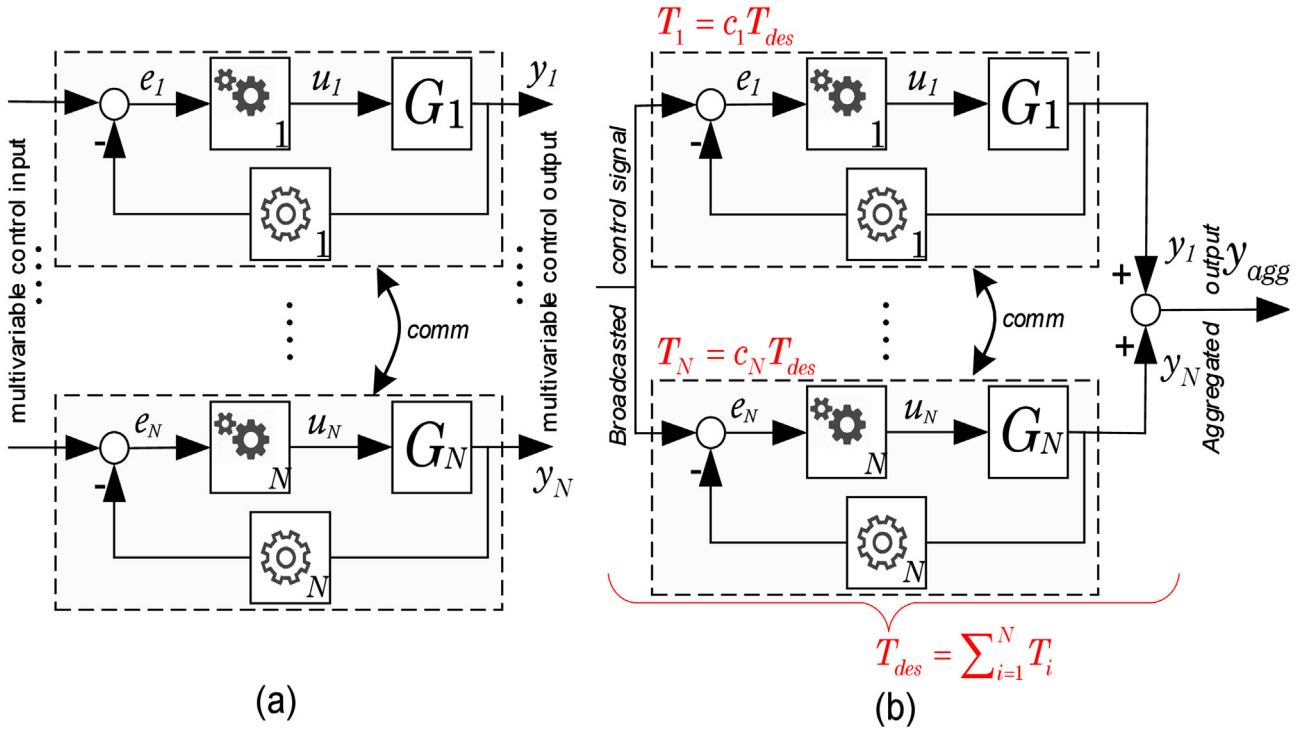


FIGURE 2 Prototypical DVPP control methods. (a) Multivariable centralized control. (b) Common variable decentralized control

The above equation is also depicted graphically in Figure 3a. If there exists an optimal desired specification, T_{des} for the DVPP such that, $y_{agg}^* = T_{des} \cdot u$, then, segregating it in P and Q class inputs, the following is obtained;

$$y_{agg}^* = \tilde{T}_{des} \cdot \tilde{u}, \quad (11)$$

where $\tilde{T}_{des} = \begin{bmatrix} T_{des}^P & 0_{1 \times K} \\ 0_{1 \times J} & T_{des}^Q \end{bmatrix}$ and $T_{des}^P = \mathbb{P}(T_{des})$, $T_{des}^Q = \mathbb{Q}(T_{des})$.

The aggregated output (y_{agg}) of the uncontrolled DVPP in Equation (10), can be reinforced to follow/match the desired output (y_{agg}^*) given in Equation (11) by implementing the appropriate control at the aggregated DVPP level, satisfying the following;

$$\tilde{T}_{des} = \left(\sum_{i=1}^N \tilde{G}_i \right)^{RC}, \quad (12)$$

where the superscript ' RC ' stands for reinforce-control at the aggregated DVPP level. The desired specification in LHS in Equation (12) can be achieved if it could be disaggregated to the individual units following the decentralized reinforce-control for each unit. In other words, the superscript ' RC ' in Equation (12) can be decentralized to the unit level, that is, $\tilde{G}_i^{rc_i}$ if LHS can be disaggregated. The solution approach for this to happen is introduced next by inventing the PF for disaggregation.

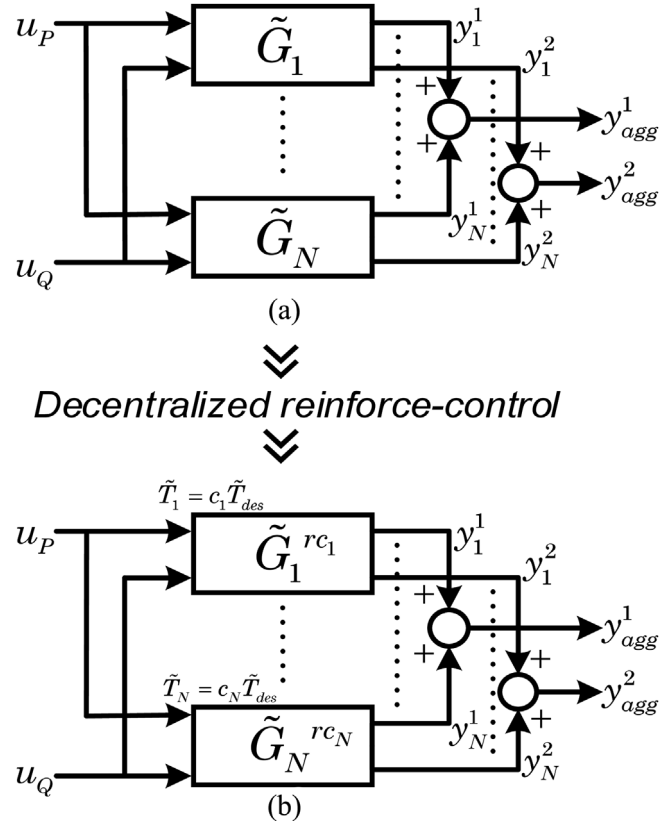


FIGURE 3 (a) Uncontrolled-DVPP. (b) Controlled-DVPP following decentralized reinforce-control

4 | DECENTRALIZED REINFORCE-CONTROL BY INVENTING AND ADOPTING THE PFs: SOLUTION APPROACH

The solution approach to achieve the objective given in Equation (12) can be divided into two steps;

- (i) Disaggregation and weighted pooling: PF invention
- (ii) Decentralized reinforce-control for matching disaggregated specification (local model-matching)

4.1 | Disaggregation and weighted pooling: PF invention

In this first step, the DVPP specification (LHS in Equation 12) is disaggregated to every unit in a robust fashion as follows;

$$\tilde{T}_{des} = \sum_{i=1}^N \tilde{T}_i = \sum_{i=1}^N c_i \cdot \tilde{T}_{des}, \quad (13)$$

where \tilde{T}_i is a disaggregated specification for i^{th} unit of DVPP and each c_i is a TF, termed as PF which follows the criterion of weighted pooling as signified by Equation (13), that is,

$$\sum_{i=1}^N c_i = 1, \quad (14)$$

$$\Rightarrow \tilde{T}_i = \left(\frac{c_i}{\sum_{i=1}^N c_i = 1} \right) \cdot \tilde{T}_{des}. \quad (15)$$

Now that the DVPP-specification is disaggregated to N DVPP's units (Equation 13), the overall reinforce-control (RHS of Equation 12) can also be decentralized to N DVPP's units as follows;

$$\left(\sum_{i=1}^N \tilde{G}_i \right)^{RC} = \sum_{i=1}^N (\tilde{G}_i)^{rc_i}, \quad (16)$$

where the superscript rc_i represents the decentralized reinforce-control to i^{th} unit which will ensure i^{th} unit to meet the disaggregated specification, \tilde{T}_i , as expressed below;

$$\tilde{T}_i = c_i \cdot \tilde{T}_{des} = (\tilde{G}_i)^{rc_i} \quad \forall i \in [1 N]. \quad (17)$$

The uncontrolled unit's output given by Equation (9), after decentralized reinforce-control can be written as;

$$y_i = (\tilde{G}_i)^{rc_i} \cdot \tilde{u}, \quad (18)$$

and finally, the output, y_i from N controlled units can be pooled to get the aggregated output as desired (Equation 11), that is,

$$y_{agg}^* = y_{agg} = \sum_{i=1}^N y_i = \sum_{i=1}^N (\tilde{G}_i)^{rc_i} \cdot \tilde{u}. \quad (19)$$

The transformation of uncontrolled DVPP constituted by the uncontrolled units (Equation 10) into the controlled DVPP constituted by the controlled units (Equation 19), is also picturised in Figure 3b.

Notice that, for SISO control, Figure 3b would become reminiscent of Figure 2b. Though we have presented the DVPP theory and its control objective in generalized MIMO system/control form in this section, further study in this article is limited to SISO system/control. For this objective of decentralized reinforce-control (Equation 19), we choose two degrees of freedom internal model control (2DOF-IMC), which could also be applicable in a MIMO control system.

4.2 | Decentralized reinforce-control: Local model matching

Decentralized reinforce-control is implemented by adopting the 2DOF-IMC technique in this article which will resemble the control structure as shown in Figure 2b wherein, two controllers are equipped with each unit in a feedforward and feedback loops to regulate the error e_i such that the unit is reinforced to follow the disaggregated specification, $T_i = c_i T_{des}$. But, before illustrating 2DOF-IMC, 1DOF-IMC is discussed next for better stepwise understanding.

4.2.1 | Brief on 1DOF-IMC and its infeasibility for dissimilar input-output

Over the years, the IMC approach and its modifications have been reported persistently in various process control applications in diverse research fields including load frequency control (droop), inverter-control etc. [39–45]. IMC has been proven to be a robust, less computational, sub-optimal, and easily understandable control method [39, 45]. The authors have enhanced the control performance of the grid-connected PV system by using IMC wherein, the PI and IMC controls are implemented in cascade with PI being in DC link voltage control, and IMC being in current control [44]. The authors in Ref. [43] have shown the outperformance of 1DOF-IMC control over proportional-resonant control in controlling the inner loop (current) for a single-phase grid-connected voltage source inverter. The authors in [45], have designed an IMC for fractional-order plus time derivative (FrOPTD) process, meeting the desired gain & phase margin independently, and also have shown its comparison with standard IMC utilizing the DC servo-system testbed.

The standard IMC structure is shown in Figure 4a which is also referred to as 1DOF-IMC structure [42]. \tilde{G}_i is an approximated or internal/reduced model of the i^{th} unit, G_i , and D_i is the output disturbance model. u_i & y_i are the local input and local output, respectively. The error, e_i , represents the effect of disturbances and plant/model mismatch which is regulated by controller, Q_i and u_{brd} is a globally broadcasted control input in perspective to DVPP.

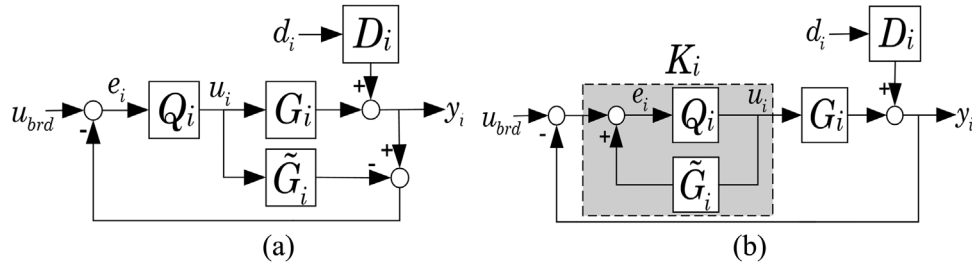


FIGURE 4 (a) Standard 1DOF-IMC structure. (b) Classical restructuring of 1DOF-IMC

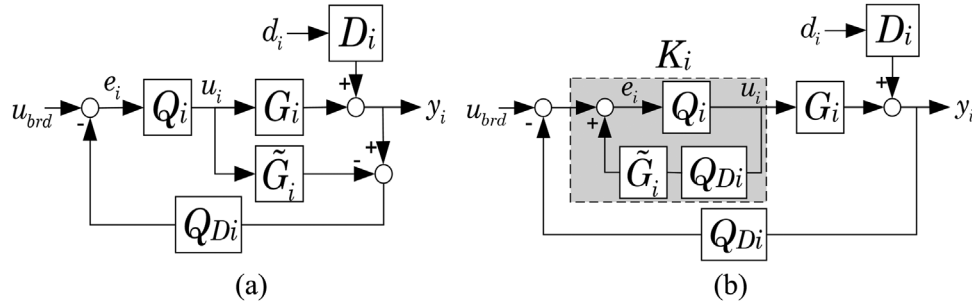


FIGURE 5 (a) 2DOF-IMC structure. (b) Classical restructuring of 2DOF-IMC

This IMC structure can be restructured in the form of a classical control structure as shown in Figure 4b. It can be observed that the error, e_i to the controller, Q_i in Figure 4a and 4b is the same, that is, $e_i = u_{brd} - y_i + \tilde{G}_i \cdot u_i$, as both the structures are mathematically the same. From this equation and Figure 4b, it can be observed that this control structure involves direct subtraction of input, u_{brd} and output, y_i , therefore the application of standard 1DOF-IMC is limited to the set-point tracking control problems only, and thus it is not suitable for dissimilar input-output. As a solution, the researchers utilize the upgraded/modified version of 1DOF-IMC, that is, 2DOF-IMC for its reasonable application in plant control with dissimilar input-output [39, 41] bringing more robustness in the control.

4.2.2 | Implementation of 2DOF-IMC for decentralized reinforce-control

In 2DOF-IMC, a secondary controller is equipped in the structure, and depending on its location, many 2DOF-IMC structures have been reported in the literature. Authors in [39–41], have utilized the 2DOF-IMC for load frequency control (droop control) problem, which involves two dissimilar input-output with input being mechanical power and output being frequency. As discussed before, DVPP's units also involve two dissimilar input-output with input being the frequency and output being the active power. The selected 2DOF-IMC structure to carry out the study is shown in Figure 5a [41, 42] and its restructuring (classical) is shown in Figure 5b. It is noteworthy here that the control structure in Figure 5b is reminiscent of the unit control structure shown in Figure 2b wherein, the

controller, K_i is a feedforward controller and the controller Q_{D_i} is the feedback controller.

Consider a local power-frequency (p-f) relation of any i^{th} commercial unit (uncontrolled) in the DVPP, either converter-interfaced or converter-less as follows;

$$y_i = G_i \cdot u_i, \quad (20)$$

$$\ni \left| \lim_{s \rightarrow 0} G_i \right| = k_{d_i}, \quad (21)$$

where u_i and y_i are the local frequency input and power output, respectively, and $k_{d_i} = \frac{1}{r_i}$ is the droop gain with r_i being the droop coefficient.

In a realistic situation, where $\tilde{G}_i \neq G_i$ and $D_i \neq 0$, the structures shown in Figure 5 can be represented mathematically by the following equations;

$$y_i = G_i \cdot u_i + D_i \cdot d_i, \quad (22)$$

$$e_i = u_{brd} - Q_{D_i} \cdot y_i + Q_{D_i} \cdot \tilde{G}_i \cdot u_i, \quad (23)$$

$$u_i = Q_i \cdot e_i, \quad (24)$$

$$\ni \lim_{s \rightarrow 0} Q_{D_i} = \frac{1}{\left| \lim_{s \rightarrow 0} G_i \right|} = r_i. \quad (25)$$

Eliminating u_i and e_i from Equations (22)–(24), output, y_i is obtained as;

$$y_i = \frac{G_i \cdot Q_i}{1 + (G_i - \tilde{G}_i) \cdot Q_i \cdot Q_{D_i}} \cdot u_{brd} + \frac{(1 - \tilde{G}_i \cdot Q_{D_i} \cdot Q_i) \cdot D_i}{1 + (G_i - \tilde{G}_i) \cdot Q_i \cdot Q_{D_i}} \cdot d_i, \quad (26)$$

$$\Rightarrow y_i = \frac{G_i \cdot K_i}{1 + G_i \cdot K_i \cdot Q_{D_i}} \cdot u_{brd} + \frac{D_i}{1 + K_i \cdot G_i \cdot Q_{D_i}} \cdot d_i, \quad (27)$$

where

$$K_i = \frac{Q_i}{1 - \tilde{G}_i \cdot Q_{D_i} \cdot Q_i}, \quad (28)$$

is a representation of a classical controller as highlighted in Figure 5b which is derived from the two IMC controllers, Q_i & Q_{D_i} . Further, Equation (27) can be written as;

$$y_i = \eta_i \cdot u_{brd} + \varepsilon_i \cdot d_i, \quad (29)$$

where $\eta_i = \frac{G_i \cdot K_i}{1 + G_i \cdot K_i \cdot Q_{D_i}}$ is the complementary sensitivity (or transmissibility) TF and $\varepsilon_i = \frac{D_i}{1 + K_i \cdot G_i \cdot Q_{D_i}}$ is the sensitivity TF. Now, from Equations (17) and (18), the disaggregated specification, T_i , can be achieved in a robust fashion by achieving the following two objectives;

$$\eta_i \approx T_i, \quad (30)$$

$$\varepsilon_i \approx 0. \quad (31)$$

From Equations (29) and (30), Q_i can be obtained as;

$$Q_i \approx \frac{T_i}{G_i - (G_i - \tilde{G}_i) \cdot Q_{D_i} \cdot T_i}, \quad (32)$$

whereas, the condition for disturbance rejection can be achieved from Equations (29) and (31) as follows;

$$Q_i \approx \frac{1}{\tilde{G}_i \cdot Q_{D_i}}. \quad (33)$$

Any particular selection of Q_{D_i} cannot satisfy both Equations (30) and (31) simultaneously. Satisfying Equation (30) will lead to sacrificing Equation (31) or vice-versa. Therefore, a compromise has to be made leading to the design of an optimal controller, Q_{D_i} for robustness. If for simplicity, the measurement noise is neglected, that is, $D_i = 0$, then from Equation (27), the aggregated DVPP output can finally be obtained as;

$$y_{agg} = \left(\sum_{i=1}^N T_i \right) \cdot u_{brd} = \left(\sum_{i=1}^N \frac{G_i \cdot K_i}{1 + G_i \cdot K_i \cdot Q_{D_i}} \right) \cdot u_{brd}. \quad (34)$$

Notice that the target of decentralized reinforce-control represented by superscript ' n_i^d ' in Equation (19) is achieved in

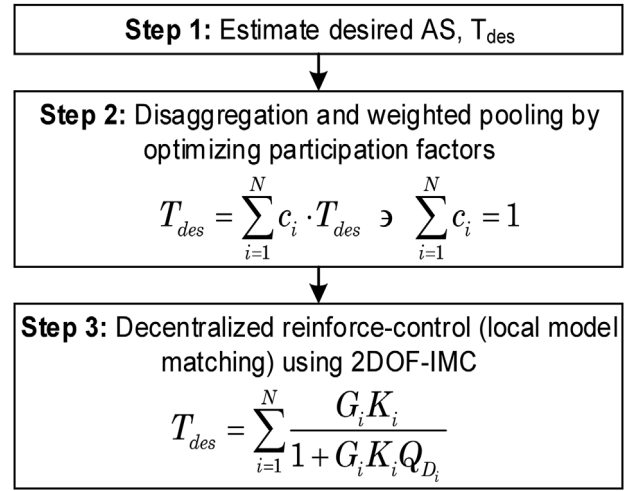


FIGURE 6 Highlights of the solution approach

Equation (34) which is also a mathematical representation of Figure 2b.

In an unrealistic ideal situation where $\tilde{G}_i = G_i$, the controller Q_i can be obtained from Equation (32) as follows;

$$Q_i = G_i^{-1} \cdot T_i, \quad (35)$$

thus, K_i in Equation (28) will become as follows;

$$K_i = \frac{Q_i}{1 - Q_{D_i} \cdot T_i}. \quad (36)$$

The highlights of the solution approach explained in this section are depicted in the flow chart in Figure 6.

5 | ASSUMPTIONS, CAUSALITY, AND PFs: DISCUSSION

5.1 | Assumptions

The following assumptions are considered while incorporating the control technique for the presented ideal case studies in this article.

Assumption-1: In Equation (13), the PF, c_i is chosen such that the desired disaggregated specification is achievable by the individual unit, that is,

$$\tilde{T}_i = c_i \cdot \tilde{T}_{des} \in \mathcal{T}_i, \quad (37)$$

where \mathcal{T}_i is an achievable unit-level set of constraints. For example, \mathcal{T}_i may include formalization of achievable domain/range of closed-loop cross-over frequencies, that is, $\mathcal{T}_i(j\omega) \subset \mathcal{C}_i(j\omega)$, $\forall \omega \geq 0$ with \mathcal{C}_i being the domain of closed-loop controlled unit or it may include energy reserve capacity.

Assumption-2: The DVPP's desired specification, \tilde{T}_{des} is achievable within the aggregated constraint formed by all constituent

individual units, that is,

$$\tilde{T}_{des} \in \sum_{i=1}^N \mathcal{T}_i. \quad (38)$$

5.2 | Causality discussion

Closed-loop stability can be guaranteed only if \mathcal{Q}_i in Equation (28) is causal and stable [39, 43]. In case of non-causality of \mathcal{Q}_i , the desired DVPP specification, T_{des} can be re-specified as, $\frac{T_{des}(s)}{(1+sT)^m}$, where $\frac{1}{(1+sT)^m}$ with $T > 0$ is a low-pass filter of sufficiently high order, m so that \mathcal{Q}_i in Equation (28) becomes a causal TF. This filter can also be a fractional-order filter, that is, $\frac{1}{1+sT^m}$, as used in Ref. [45] for ensuring causality. For a very good approximation (reduced model), G_i must be invertible [42] for stable \mathcal{Q}_i which precludes among unstable zeros of G_i . In the case of a nonminimum phase system, it can be factorized in its minimum phase and nonminimum phase part as: $G_i = G_{i-} \cdot G_{i+}$ and then the inverse can be approximated from its nonminimum phase part as: $G^{-1} = (G_{-})^{-1}$ to obtain the stable \mathcal{Q}_i [39]. Alternatively, there is also a headroom through c_i in choosing individual T_i to make \mathcal{Q}_i causal and stable.

5.3 | Exemplifying the PFs

This section exemplifies the possible choices that could be made for PFs. One possible example for DVPP could be a wind power park wherein, all units are wind generators operating for FCAS with the desired specification as $T_{des}(s) = \frac{Ms+D}{1+Ts}$ where $M, D > 0$ are the desired virtual inertia and damping coefficient, respectively, and the denominator $1 + Ts$ with $T > 0$ is included as a low-pass filter. If each turbine has a power rating, $r_i > 0$, the PF can be selected in the scalar form as $c_i(s) = \frac{r_i}{\sum_{i=1}^N r_i}$. It is noteworthy here that this choice of PF became analogous to the traditional droop control architecture.

In another possible example of DVPP consisting of hydro plant, BESS, and supercapacitor (SC), the following choices for c_i s could be made.

- (i) **Low-pass filter:** For RES, such as hydro-generator with low bandwidth and NPB that are limited in power but rich in energy, the choice of PF could be as, $c_i(s) = \frac{\mathcal{K}_i}{1+sT_i}$ where T_i is a time constant in a high range which will assign the slow dynamics to the hydro-generator.
- (ii) **High-pass filter:** For ESS, such as SCs with high bandwidth, able to inject quickly with high-power capacity but limited in energy, the choice of PF could be as $c_i(s) = \frac{s\mathcal{K}_i}{1+sT_i}$ where T_i is a time constant in low range for assigning fast dynamics.
- (iii) **Band-pass filter:** For ESS, such as BESS which is able to cover the intermediate bandwidth between the above

two, the choice of PF could be as $c_i(s) = \frac{s\mathcal{K}_i}{(1+sT_{1,i})(1+sT_{2,i})}$ where $T_{i,1}$ & $T_{i,2}$ are the lower and upper time constant, respectively.

6 | TEST SYSTEM

6.1 | Western system coordinating council (WSCC) test system

The test system considered in this article is ‘western system coordinating council (WSCC)’ (IEEE 3-machine, 9-bus) system with a 100 MVA base, the single line diagram of which is shown in Figure 7. The needful details are depicted in the same figure including loads and generations values. The line numbers are depicted in such a manner that if the depicted line number is placed more towards i^{th} bus instead of in the middle of i^{th} and j^{th} bus then it means that the line is from i to j . The foundation data is presented in Ref. [46]. It consists of three thermal generators connected at Bus nos. 1–3, respectively, six constant impedance transmission lines and 3 loads connected at Bus nos. 5–8, respectively. The generations by G1-G3 are at the base level of 16.5 kV, 18 kV, and 13.8 kV, respectively, whereas the transmission is at the base level of 230 kV. A complete interconnected WSCC system can be represented by the following differential-algebraic equations [47];

$$\dot{X} = f(X, X^{alg}, U), \quad (39)$$

$$0 = g(X, X^{alg}, U). \quad (40)$$

The variable, X represents the set of ‘state variables’ such as: rotor angle (δ), angular speed (ω), regulator’s states etc., whereas X^{alg} represents the set of ‘algebraic variables’ such as: bus voltage (V_m) and its angle (θ) [47]. The variable, U is an exogenous input. By solving the load-flows for the system (Equation 40), the operating point, (X_0, X_0^{alg}, U_0) can be acquired. Eliminating algebraic variables and linearizing them around the operating point, (X_0, U_0) , the state-space model of the system (Equation 39) for the defined output, Y can be obtained as follows [47];

$$\Delta \dot{X} = A\Delta X + B\Delta U, \quad (41)$$

$$\Delta Y = C\Delta X + D\Delta U, \quad (42)$$

where A is the state/system matrix and B, C, D are the input, output, and feedforward matrices, respectively.

Each generator in the WSCC system (Equations 41 and 42) is modelled as fourth-order Heffron & Phillips model similar to in Ref [47, 48] which is equipped here with ‘3rd order generic TG’ [46, 49] in mechanical torque loop. Figure 8 shows the TG model which assimilates the droop control through the droop coefficient as shown in Figure 8.

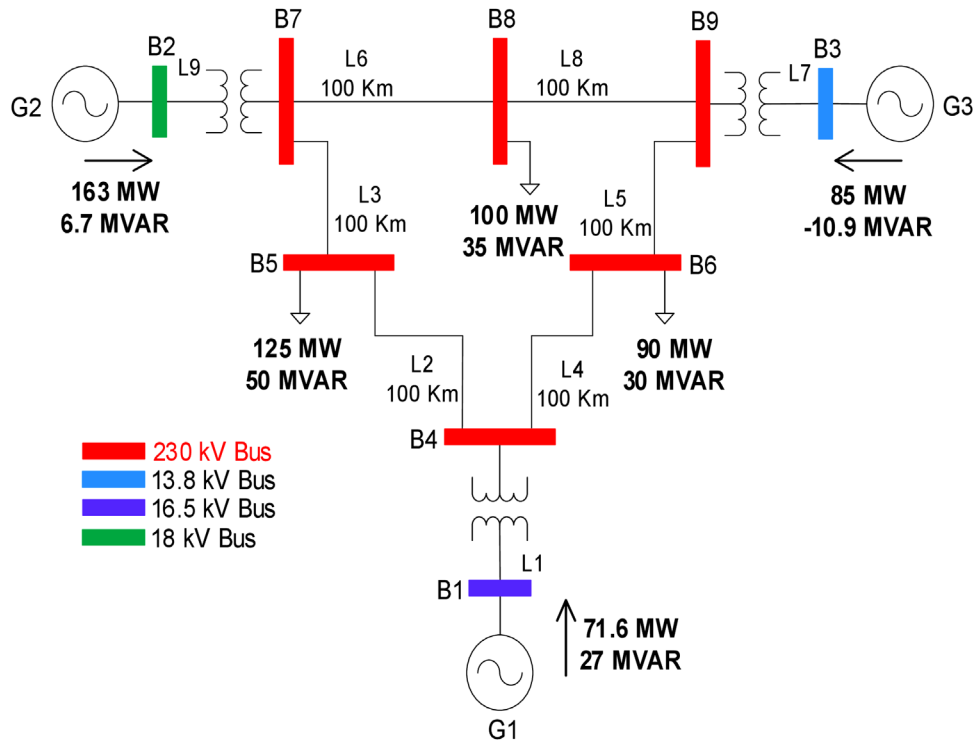


FIGURE 7 WSCC test system

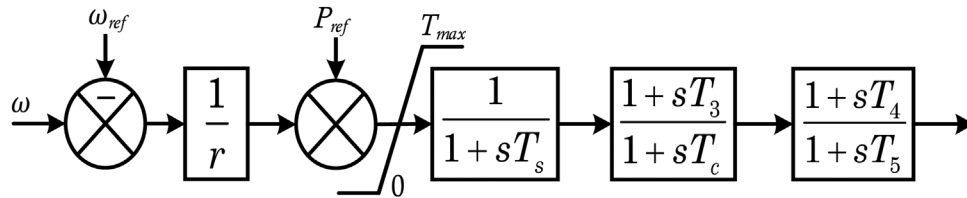


FIGURE 8 Generic TG system of thermal generator

The TF of the TG is given in Equation (43) wherein, the subscripts, ‘*t*’ and ‘*m*’ signify thermal and mechanical, respectively, and the parameters are given in Table A1. The ‘3rd order IEEE DC type 1 exciter’ [48] is equipped with only G2. For the specific operating point depicted in Figure 7, the LTI system (Equations 41 and 42) is obtained using the PST toolbox [46].

$$G_{t,m}(s) = \frac{1}{r} \cdot \left(\frac{1}{1+sT_s} \right) \cdot \left(\frac{1+sT_3}{1+sT_c} \right) \cdot \left(\frac{1+sT_4}{1+sT_5} \right). \quad (43)$$

6.2 | DVPP constituents

DVPP, which is planned to substitute the thermal generator in the test system (Figure 7), encompasses a RES unit and ESS units.

6.2.1 | RES unit

Despite its low relative inertia, the hydro plant is reported to be the best choice to seek various ASs from [21, 50]. SRAS, voltage control AS, network loading control AS, PFCAS, and SFCAS are some very common ASs being provided by the hydro plant [21, 50]. With the assistance of ESSs, the capability of the hydro plant can further be strengthened for FFCAS and PFCAS [7, 21] to reduce the impact of its low-inertia and NPB. Therefore, the hydro-generator is selected as a RES-constituent of DVPP. It is known that an approximate hydro-generator model differs from an approximate thermal generator model majorly on two fronts, that is, TG and inertia constant. Therefore, the hydro-generator is achieved from the same thermal generator data [46] by changing its TG to ‘5th order IEEE type 3’ [48] and by reducing the inertia constant. The hydro TG is shown in Figure 9 and its TF is given in Equation (44) wherein, the subscript ‘*b*’ signifies hydro and the parameters are given in

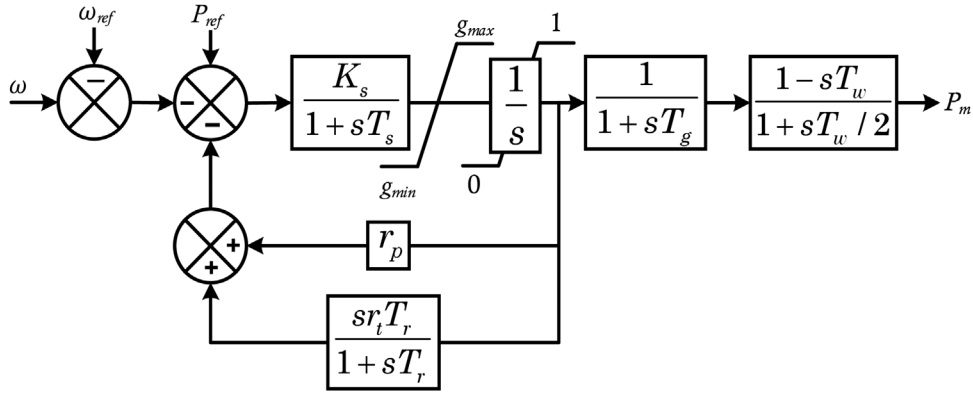


FIGURE 9 IEEE type 3 TG model of hydro generator

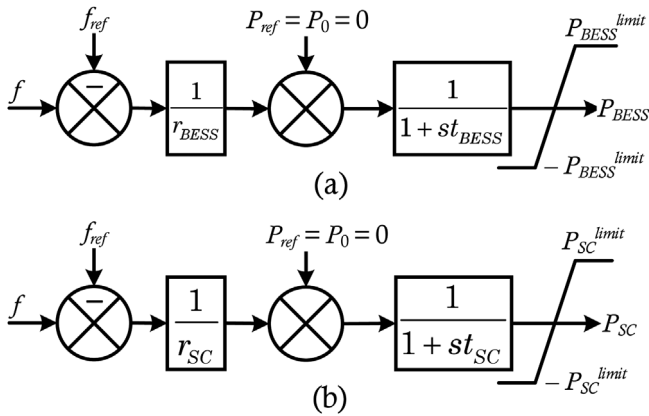


FIGURE 10 Generic droop controlled model of (a) BESS and (b) SC

Table A1.

$$G_{h,m}(s) = \left(\frac{K_s(T_r s + 1)}{T_r T_s s^3 + (T_r + T_i) s^2 + T_r (r_p + r_i) s + K_s r_p} \right) \cdot \left(\frac{1}{1 + T_g s} \right) \cdot \left(\frac{1 - s T_w}{1 + s \frac{T_w}{2}} \right). \quad (44)$$

6.2.2 ESS units

BESS has a wide-range ability (slow to fast) to provide FCAS by regulating the active power at the PCC and thus, has been proven very effective in practical applications as a solution to low-inertia power systems [13, 20, 21, 24] in the form of ASs. With sufficient storage reserve, it can contribute to both, that is, PFCAS+FFCAS. The time constant of BESS can be small enough to share the fast dynamics but then, the lifespan and efficiency will be compromised. Therefore, SC is placed as a third constituent unit in DVPP which will be assigned with fast dynamics and thus, will help in limiting the stress and temperature on/of BESS resulting in its better life-span and efficiency. A droop-controlled converter-interfaced BESS and SC can be modelled as a first-order system as shown in Figure 10 [51]. In

this article, a similar model is considered for both, BESS and SC, that is, $T_{batt} = T_{SC}$ & $r_{batt} = r_{SC}$ but the control will be so as to assign fast dynamics to the SC and slow dynamics to BESS.

7 | CASE STUDY: FCAS

7.1 | Problem formulation for net-zero targets

The electrical power of the largest thermal generator, G_1 (therm-G1) in the test system (Figure 7) can be obtained from Equation (2) as follows;

$$\dot{p}_{t,e}^1 = \dot{p}_{t,m}^1 - \frac{2H_t^1}{f_n} \frac{df_1}{dt}, \quad (45)$$

where H_t^1 is inertia constant of a therm-G1 and subscripts 'e', signifies electrical and 'm', 'r' signifies same as before. Following the TG's frequency response model [52], the above Equation (45) can further be written in the linearized frequency domain as;

$$\Delta \dot{p}_{t,e}^1(s) = \underbrace{G_{t,m}^1(s) \cdot (-\Delta f_1(s))}_{TG \text{ response}(PFCAS)} - \underbrace{\frac{2H_t^1}{f_n} s \cdot \Delta f_1(s)}_{IR(FFCAS)}, \quad (46)$$

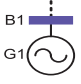
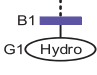

where,

$$G_{t,m}^1(s) = \frac{\Delta \dot{p}_{t,m}^1(s)}{-\Delta f_1(s)}, \quad (47)$$

is a TG's TF of therm-G1 (see Equation 45) with $\Delta \dot{p}_{t,m}^1(s)$ being the mechanical power input to the shaft. In per unit study with $f_n = 1$, the TF for electrical power of therm-G1, $G_{t,e}^1(s)$ just after the frequency excursion event, that is, in PFCAS+FFCAS region, can be obtained from Equation (46) as;

$$G_{t,e}^1(s) = \frac{\Delta \dot{p}_{t,e}^1(s)}{\Delta f_1(s)} = - (G_{t,m}^1(s) + 2H_t^1 s). \quad (48)$$

TABLE 1 Formation of case study

Case. No.	Description	Graphical depiction at Bus-1
1.	Default system with $H_b^1 = 23.64$ $t_b^1 = 10.70$	
2.	Hydro-G1 with $H_b^1 = 5.64$ $t_b^1 = 18.51$	
3.	DVPP for only PFCAS encompassing Case-2	
4.	DVPP for PFCAS+FFCAS encompassing Case-2	-do-

Now, with the aim of net-zero targets, therm-G1 is planned to be substituted with a hydro-generator, G_1 (hydro-G1) having the same generation and rating. The TF for electrical power of hydro-G1, $G_{b,e}^1(s)$ can be derived in a similar manner as;

$$G_{b,e}^1(s) = \frac{\Delta p_{b,e}^1(s)}{\Delta f_1(s)} = - \left(G_{b,m}^1(s) + 2H_b^1 s \right), \quad (49)$$

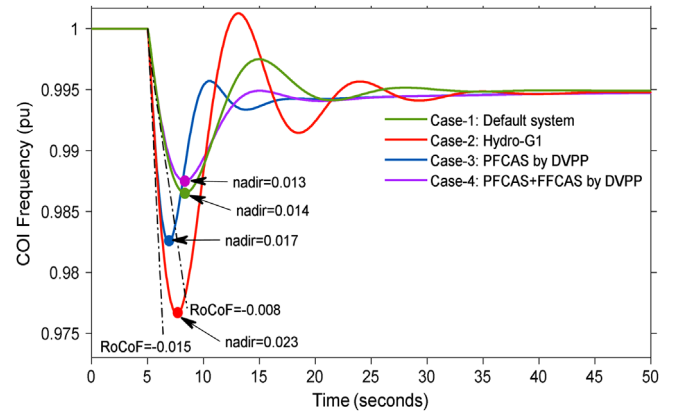
where $G_{b,m}^1$ and H_b^1 are the TG's TF (see Equation 46) and inertia constant of hydro-G1, respectively, with $H_b^1 < H_t^1$ and $t_b^1 > t_t^1$ where, t denote the TG's response time.

Hydro-G1 alone cannot meet the dynamic response similar to therm-G1 due to slow TG/PFR and low IR as discussed before. Therefore, now it is required to seek ASs in the system for PFR and IR restoration for which, the DVPP constituted in Section 6.2 is implemented. Hydro-G1 has been made one of the constituents of DVPP. The system shown in Figure 7 will be studied under three cases as listed in Table 1.

The adverse impact of slow PFR and low IR (Case-2) will be discussed and counteracted in Cases 3–4 which correspond to next sections. Frequency nadir/zenith and RoCoF being the key metrics of PFR and IR, respectively [52, 53], are utilized for the analysis in the next sections. It is mentioned before that, the RoCoF is a function of two factors, (1) inertia constants and (2) net power imbalance or load disturbance. It is also noteworthy here that the frequency nadir is also a function of these two factors in addition to a third factor, (3) TG's response [52].

7.2 | Restoration of PFR by DVPP: PFCAS

Cases 1–2 are simulated subjected to step load increment of 50 MW at load bus, B6, and the needful responses are shown in Figures 11–12. Referring to Figure 11, the COI frequency (Equation 4) is utilized to analyse the system through RoCoF and frequency nadir metrics. Following Ref. [54], RoCoF metric is considered as a minimum value of instantaneous RoCoF in the first 500 ms from the start of the frequency excursion event,

**FIGURE 11** COI frequency for all Cases 1–4.

that is,

$$RoCoF = \min \left(\frac{df_c(t)}{dt} \right) \quad \forall t \in [t_{event} \ t_{event} + 500ms]. \quad (50)$$

It can be seen in Figure 11 that RoCoF and frequency nadir are degraded in Case-2 in comparison to Case-1 which suggests the need for PFCAS and FFCAS to restore PFR and IR, respectively. Reasons for this degradation can be ascertained from Figure 12a, plotted for electrical power response, and from Figure 12c, plotted for mechanical power response. It can be observed that the power response of hydro-G1 (Case-2) has become poor than Case-1 due to two factors: (1) slow TG/PFR with NPB (2) lower inertia-constant/IR, resulting in a degradation of RoCoF and frequency nadir. The response for reactive power injections at bus 1 are also plotted in Figure 12b for all four Cases given in Table 1 however, DVPP units are not controlled additionally for reactive power injections in Case 3–4. But, the generators including the untouched hydro generator/unit of DVPP would still respond to voltage dip caused by step load (active) increment as per the dynamics of synchronous generators. Further discussion on reactive power is omitted as the voltage control study is out of the scope of this article.

Firstly, the restoration of PFR is focused only (Case-3) in this section by providing only PFCAS from DVPP at B1. As per the

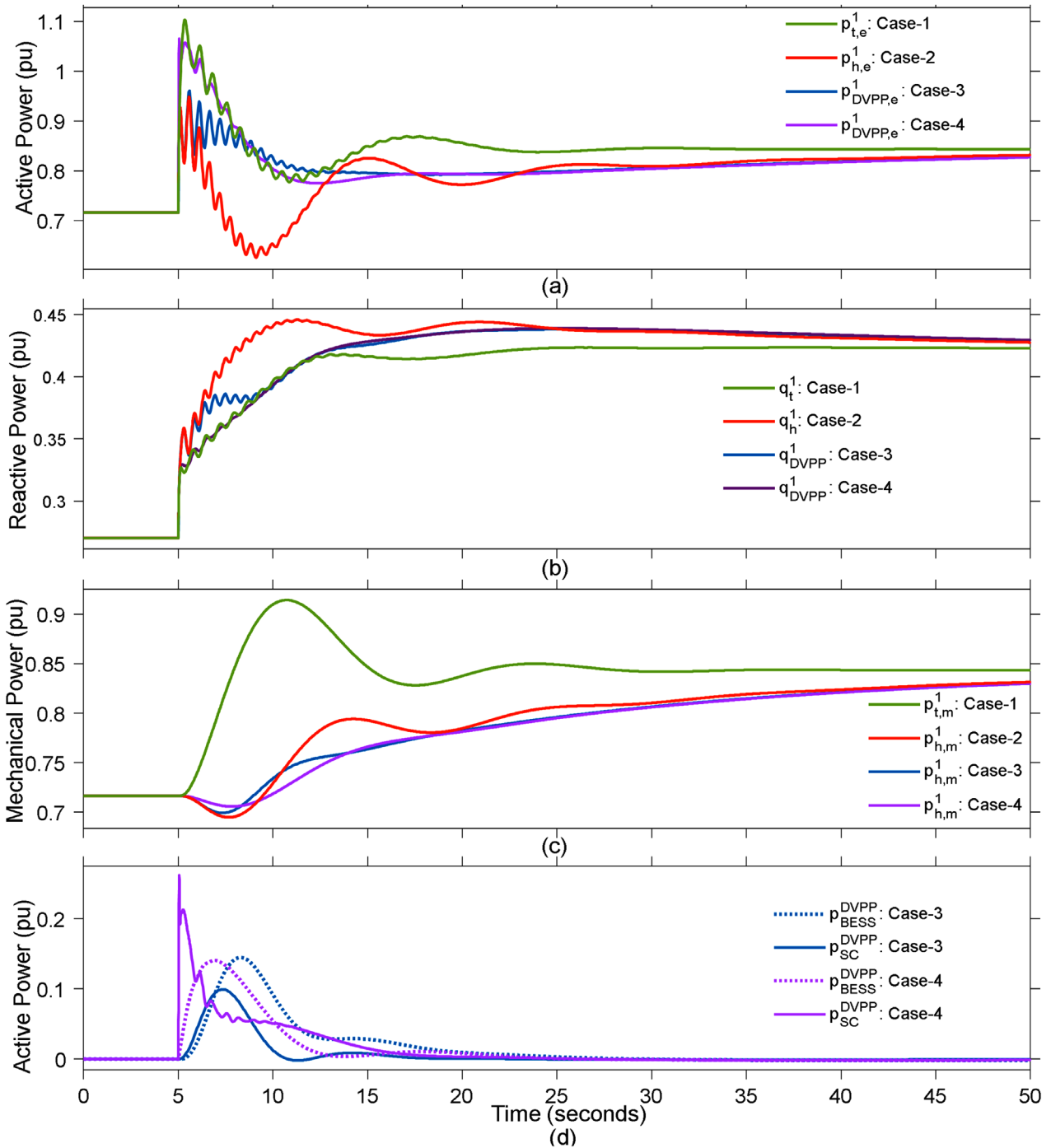


FIGURE 12 Power injections at B1 for all Cases 1–4. (a) Active power, (b) reactive power, (c) mechanical power, (d) active power by DVPP's storage constituents

flow chart in Figure 6, the solution approach adopted for Case-3 is illustrated below;

Step-1: The approach is kicked off by selecting the desired specification, T_{des} at B1 which is kept equal to the TF for electrical power of therm-G1, $G_{t,e}^1(s)$ as given in Equation (48). But, PFCAS being the only focus here, the IR part, that is, $2H_t^1 s$ is dropped in T_{des} reducing it to;

$$T_{des}(s) = -G_{t,m}^1(s). \quad (51)$$

Step-2: In this step, the PFs for each unit in the DVPP are required to be optimized in order to disaggregate above T_{des} such that the following holds true;

$$\begin{aligned} T_{des}(s) &= T_{hydro}(s) + T_{BESS}(s) + T_{SC}(s) \\ &= c_{hydro}(s) \cdot T_{des}(s) + c_{BESS}(s) \cdot T_{des}(s) \\ &\quad + c_{SC}(s) \cdot T_{des}(s), \end{aligned} \quad (52)$$

$$\ni c_{hydro}(s) + c_{BESS}(s) + c_{SC}(s) = 1. \quad (53)$$

Though the disaggregated specification for hydro-G1, that is, $T_{hydro} = c_{hydro} \cdot T_{des}$ can be set by appropriate selection of c_{hydro} and then the plant can be reinforced to match the same, in this article, the hydro-G1 is planned to remain untouched (same as in Case-2), that is, without decentralized reinforce-control which can be made possible if the following holds true for Equation (52);

$$T_{hydro}(s) = c_{hydro}(s) \cdot T_{des}(s) = -G_{b,m}^{-1}(s). \quad (54)$$

Referring to Equation (49), notice that the IR part of hydro-G1, that is, $2H_b^1 s$ is also dropped in above Equation (54) for the same reason as mentioned in step 1. In other words, T_{des} for DVPP in Equation (51) is a TF for mechanical power of DVPP, that is, $T_{DVPP,m}$. It is also noteworthy that, even though T_{BESS} and T_{SC} are the TFs for electrical powers in Equation (52) but, are also compensating/assisting the mechanical power deficit incurred by slow and NPB of hydro TG. Nonetheless, the TF for electrical power of DVPP, that is, $T_{DVPP,e}$ can be obtained as follows;

$$\begin{aligned} T_{DVPP,e}(s) &= T_{DVPP,m}(s) + T_{DVPP,l}(s) \\ &= T_{des}(s) + 2H_b^1 s. \end{aligned} \quad (55)$$

In the particular case study here, instead of assigning slow dynamics to hydro-G1 through optimized c_{hydro} , we are actually estimating it from Equation (54) using the already existing slow hydro-G1 (T_{hydro}) and thus c_{hydro} can be obtained as (see Appendix);

$$\begin{aligned} c_{hydro}(s) &= \frac{-G_{b,m}^{-1}(s)}{T_{des}(s)} = \frac{-G_{b,m}^{-1}(s)}{-G_{t,m}^{-1}(s)} \\ &= \frac{-3.81 (s - 0.37) (s + 0.2) (s + 2) (s + 10)}{(s + 13.67) (s + 5.49) (s + 0.8) (s + 0.75) (s + 0.13)}. \end{aligned} \quad (56)$$

Notice that, already existing c_{hydro} in above equation has higher order than its typically exemplified pattern/order in Section 5.3 and therefore the order of c_{BESS} and c_{SC} may also rise to upheld Equation (53). Also, the already existing c_{hydro} has a nonminimum part, obtained due to nonminimum phase behaviour of T_{hydro} in Equation (54) which may affect the causality of c_{BESS} and c_{SC} to be optimized unless taken care off. The following rules are set up to optimize c_{BESS} and c_{SC} .

(i) weighted pooling criterion given in Equation (14) is upheld, that is, c_{hydro} (fixed from Equation 56) $+ c_{BESS} + c_{SC} = 1$.

$$(ii) \frac{d}{d\omega} (20 \log |c_{BESS}(j\omega)|) = \begin{cases} +ve \text{ for } \omega < \tilde{\omega}_c \\ 0 \text{ for } \omega \cong \tilde{\omega}_c \\ -ve \text{ for } \omega > \tilde{\omega}_c \end{cases}$$

where $\tilde{\omega}_c$ is a varying centre frequency of c_{BESS} which is required to obey the pattern of a smooth bandpass filter.

(iii) Both, c_{BESS} and c_{SC} are causal and minimum phase TFs.

The PFs, c_{BESS} and c_{SC} are obtained as follows;

$$c_{BESS}(s) = \frac{3.5s (s + 10.86) (s + 2.98) (s + 0.95) (s + 0.29)}{(s + 13.67) (s + 5.49) (s + 1) (s + 0.8) (s + 0.75) (s + 0.13)}, \quad (57)$$

$$c_{SC}(s) = \frac{s (s + 14.3) (s + 5.9) (s + 0.19) (s^2 + 1.76s + 0.8)}{(s + 13.67) (s + 5.49) (s + 1) (s + 0.8) (s + 0.75) (s + 0.13)}. \quad (58)$$

The Bode plot for these three $c_i s$ are shown in Figure 13a. In this way, with the help of optimized $c_i s$, the desired specification, T_{des} is disaggregated as per Equation (52) ascertaining T_{BESS} and T_{SC} (see Appendix).

Step-3: Now, the decentralized reinforce-control as indicated in Equation (34) can be adopted for two units of DVPP, that is, BESS and SC. Referring to Figure 10, the following common model for BESS and SC is considered with a time constant, $t_{BESS} = t_{SC} = 0.02$ [51] and droop coefficient, $r_{BESS} = r_{SC} = 0.04$;

$$G_{BESS}(s) = G_{SC}(s) = \frac{1}{0.04} \cdot \left(\frac{1}{1 + 0.02s} \right). \quad (59)$$

Now, under the unrealistic situation discussed in Section 4.2.2, the controllers, Q_{BESS} and Q_{SC} can be obtained by following Equations (35) and (59), and Equations (A2) and (A3) as;

$$\begin{aligned} Q_{BESS}(s) &= G_{BESS}(s)^{-1} \cdot T_{BESS}(s) \\ &= \frac{0.35s(s+10.86)(s+2.98)(s+0.95)(s+0.29)(s+50)}{(s+13.67)(s+5.49)(s+1)(s+0.8)(s+0.75)(s+0.13)(s+10)(s+2)}, \end{aligned} \quad (60)$$

$$\begin{aligned} Q_{SC}(s) &= G_{SC}(s)^{-1} \cdot T_{SC}(s) \\ &= \frac{0.1s(s+14.3)(s+5.9)(s+50)(s+0.2)(s^2+1.76s+0.8)}{(s+13.67)(s+5.49)(s+1)(s+0.2)(s+0.75)(s+0.13)(s+10)(s+2)}, \end{aligned} \quad (61)$$

with the simple choice of $Q_{D_{BESS}} = r_{BESS} = 0.04$ and $Q_{D_{SC}} = r_{SC} = 0.04$ in Equation (36), K_{BESS} and K_{SC} can be obtained by putting Equations (60) and (61) in Equation (36), respectively. Finally, adopting the control given by Equation (34) for Equation (55), the aggregated electrical power output of DVPP, that is, $\Delta p_{DVPP,e}^1(s)$ can be obtained as follows;

$$\begin{aligned} \Delta p_{DVPP,e}^1(s) &= (T_{des}(s) + 2H_b^1 s) \cdot \Delta f_1(s) \\ &= \left\{ \left(\frac{-G_{b,m}^{-1}(s) + \frac{G_{BESS}(s) \cdot K_{BESS}(s)}{1 + G_{BESS}(s) \cdot K_{BESS}(s) \cdot Q_{D_{BESS}}(s)} + \frac{G_{SC}(s) \cdot K_{SC}(s)}{1 + G_{SC}(s) \cdot K_{SC}(s) \cdot Q_{D_{SC}}(s)}} \right) + 2H_b^1 s \right\} \cdot \Delta f_1(s). \end{aligned} \quad (62)$$

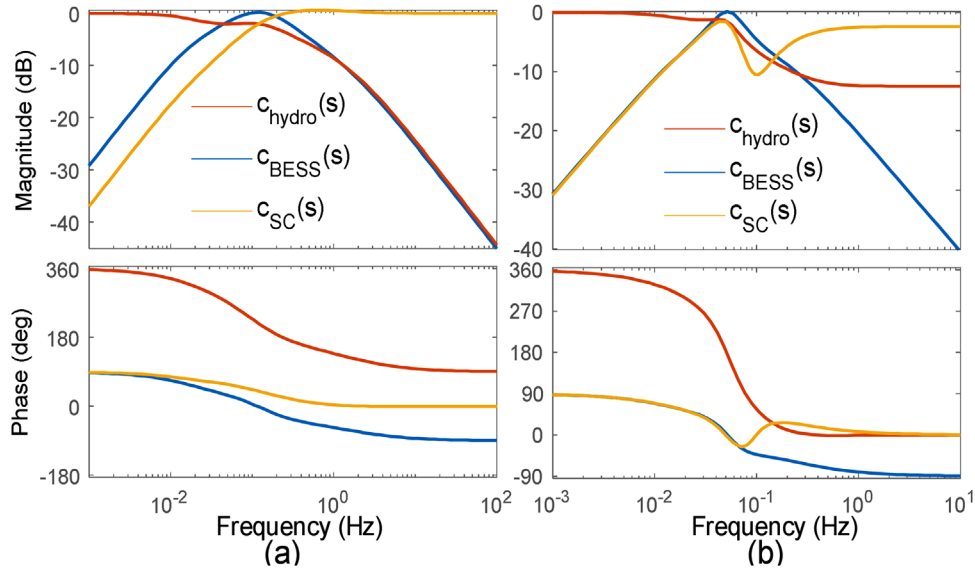


FIGURE 13 Bode plot for optimized PFs for (a) Case-3 (b) Case-4

Corresponding to this Case-3 study in this section (PFCAS only), it can be seen in Figure 11 that frequency nadir is improved than Case-2 but, still not restored back fully to Case-1 due to the lack of FFCAS (IR) from DVPP. By observing the red and blue response in Figure 12a, it can be conceived that the dynamic power response at B1 corresponding to Case-3 has been improved than what it was in Case-2 due to the supply of additional PFR by BESS and SC constituents of DVPP which are shown in Figure 12d. Notice that the hydro constituent of DVPP in Case-3 remained untouched from what it was in Case-2 that is why the mechanical power response of hydro-G1 (DVPP constituent) shown in Figure 12c for Case-3 is approximately similar to Case 2. It should also be noticed in Figure 11 that, RoCoF could not be improved due to the lack of FFCAS from DVPP and as a result, the IR by hydro-G1 remains the same for both Cases 2–3 which is reflected in initial transients of corresponding responses in Figure 12a. Thus, only PFCAS has been provided by DVPP in Case-3 leading to improve the power response and thereby frequency nadir in the PFR region only.

7.2.1 | Summary on NPB

It can be seen in Equation (46) that the hydro-generator's TG ($G_{b,m}$) is inhibiting NPB as one of the zeroes is lying in RHS. This behaviour is also reflected in the power response in Figure 12c corresponding to Case-2 (red), as it exhibits undershoot first before it starts increasing. The impact of this undershoot on mechanical power is also reflected in electrical power in Figure 12a (red). Now, by thorough observation of DVPP's output in Equation (62), it can be seen that, $-G_{b,m}^1$ (NPB) still exists in the round bracket, but when it is summed up with the other DVPP's constituents, it becomes equal to T_{des} ($-G_{t,m}^1$) which is free from NPB (see Equation 45). In other words, NPB of hydro-G1 has been internally cancelled out by

the other two constituents of DVPP. This improvement can also be seen in the electrical power response of DVPP in Figure 12a for Case-3 as the impact of undershoot is eliminated and thus, the problem of NPB is resolved as a by-product of adopted control.

7.3 | Restoration of PFR and IR by DVPP: PFCAS+FFCAS

Referring to Equation (46), most of the literature presents the study with only one FCAS, either PFCAS or FFCAS which generally needs different input signals, that is, Δf for PFCAS and RoCoF for FFCAS [55]. In this section corresponding to Case-4, it is shown how the PFCAS+FFCAS can be provided from DVPP simultaneously by utilizing only one input signal, Δf . The similar steps are executed as in the previous section with the following major changes;

Step 1: For both PFCAS and FFCAS, the T_{des} in Equation (52) will become as follows;

$$T_{des}(s) = -G_{t,e}^1(s). \quad (63)$$

Step 2: T_{hydro} in Equation (52) will become as follows;

$$T_{hydro}(s) = c_{hydro}(s) \cdot T_{des}(s) = -G_{b,e}^1(s). \quad (64)$$

c_{hydro} can be obtained from Equations (63) and (64), as follows;

$$\begin{aligned} c_{hydro}(s) &= \frac{-G_{b,e}^1(s)}{-G_{t,e}^1(s)} = \frac{G_{b,m}^1(s) + 2H_1^1 s}{G_{t,m}^1(s) + 2H_1^1 s} \\ &= \frac{0.24(s + 5.25)(s + 2)(s + 1.53)(s + 0.2)(s^2 - 0.45s + 0.14)}{(s + 5.48)(s + 1.89)(s + 0.75)(s + 0.13)(s^2 + 0.28s + 0.11)}. \end{aligned} \quad (65)$$

c_{BESS} and c_{SC} are optimized as follows;

$$c_{BESS}(s) = \frac{0.60s(s+0.43)(s^2+0.88s+0.23)}{(s+1.2)(s+0.75)(s+0.13)(s^2+0.28s+0.11)}, \quad (66)$$

$$c_{SC}(s) = \frac{0.76s(s+5.54)(s+0.92)(s+0.24)(s^2+0.36s+0.35)}{(s+5.48)(s+1.2)(s+0.75)(s+0.13)(s^2+0.28s+0.11)}. \quad (67)$$

The Bode plot for these three $c_i s$ are shown in Figure 13b. T_{BESS} and T_{SC} can be ascertained for this Case-4 as well similar as in Equations (A2) and (A3) corresponding to Case-3.

Step 3: Similar as in Case-3, Q_{BESS} and Q_{SC} are obtained as follows;

$$Q_{BESS}(s) = \frac{0.0227s(s+0.43)(s+1.89)(s+50)(s^2+0.88s+0.23)}{(s+0.75)(s+1.2)(s+2)(s+0.2)(s+0.13)}, \quad (68)$$

$$Q_{SC}(s) = \frac{0.0288s(s+5.54)(s+0.92)(s+1.89)(s+50)(s+0.24)(s^2+0.36s+0.35)}{(s+5.48)(s+0.75)(s+1.2)(s+2)(s+0.2)(s+0.13)}. \quad (69)$$

It can be seen that both controllers in Equations (68) and (69) have turned out noncausal TFs making the control technique infeasible as discussed in Section 5.2. The problem can be resolved by adding a low pass filter in cascade to both controllers as alluded in Section 5.2 leading to have the following;

$$\hat{Q}_{BESS}(s) = Q_{BESS}(s) \cdot \frac{1}{1+0.01s}, \quad (70)$$

$$\hat{Q}_{SC}(s) = Q_{SC}(s) \cdot \frac{1}{(1+0.01s)^2}. \quad (71)$$

This cultivation is likely to compromise the desired output from DVPP as per T_{des} but is minute enough to be neglected. Putting Equations (70) and (71) in Equation (36), K_{BESS} and K_{SC} can be obtained in a similar manner as in the last section. Thus, finally, $\Delta p_{DVPP,e}^1$ from DVPP is obtained as;

$$\Delta p_{DVPP,e}^1(s) = T_{des}(s) \cdot \Delta f_1(s) \cdot \left(\begin{array}{c} -G_{b,e}^1(s) \\ + \frac{G_{BESS}(s) \cdot K_{BESS}(s)}{1+G_{BESS}(s) \cdot K_{BESS}(s) \cdot Q_{DBESS}(s)} \\ + \frac{G_{SC}(s) \cdot K_{SC}(s)}{1+G_{SC}(s) \cdot K_{SC}(s) \cdot Q_{DSC}(s)} \end{array} \right) \cdot \Delta f_1(s). \quad (72)$$

Corresponding to this Case-4 study in this section, it can be seen in Figure 11 that RoCoF and frequency nadir both, have been improved up to large extent and approximately became equal to what these were in Case-1. It can be seen in Figure 12a that the power response by DVPP in Case-4 is now approxi-

mately matching what it was in Case-1 which became possible due to the additional supply from BESS and SC constituents of DVPP, which are shown in Figure 12d. From the same figure, it can be noticed that the fast dynamic due to IR demand in Case-4 has been provided by SC as planned through PF which plays important role in maintaining the BESS's efficiency and life. The resolution of NPB can also be examined similarly as examined in the last section.

8 | CONCLUSIONS

The article has introduced the DVPP from its technical perspective and the control objective has been formulated for its grid integration. The solution approach has made DVPP offer ASs in order to make its integration safe and harmless for the grid. In the first step of the solution approach, the desired specification is disaggregated among the renewable constituent units of DVPP in proportion to corresponding PFs. The disaggregated specification is then matched by implementing decentralized reinforce-control in the second step.

In the case study, the scenario of slow PFR and low IR is created in the WSCC test system by substituting the largest thermal generator with the slow and low-inertia hydro-generator, resulting in poor traditional FCAS in the system. By implementing the DVPP concept and decentralized reinforce-control for it, the PFCAS+FFCAS is provided to restore back the PFR and IR in the system which is corroborated by 'frequency nadir' and RoCoF. Thus, DVPP integration remains safe and unharmed for the grid leading to net-zero targets.

The future scope/study may cover the implementation of (1) disturbance observer-based robust IMC control (2) adaptive PFs (3) Multiple ASs (4) Intra-DVPP communication as depicted in Figure 2 for the momentary solution of DVPP's constituent's limitation or its failure.

CONFLICT OF INTEREST

No conflict of interest

PERMISSION TO REPRODUCE MATERIALS FROM OTHER SOURCES

None

DATA AVAILABILITY STATEMENT

Data sharing is not applicable to this article as no new data were created or analysed in this study.

ACKNOWLEDGEMENTS

This work is carried out under the project, 'Gridx: The Autonomous Digital Grid' funded by 'King Abdullah University of Science and Technology, Saudi Arabia' under grant OSR-2019-CoE-NEOM-4178.12 as a part of the Kingdom's vision, "New Future" and "New Enterprise Operating Model" (NEOM-2030), and Department of Library Services, University of Pretoria, South Africa.

ORCID

Lalit Kumar  <https://orcid.org/0000-0002-7715-7677>

REFERENCES

- Kraftwerke, N.: What are ancillary services? <https://www.next-kraftwerke.com/knowledge/ancillary-services>. Accessed August 2021
- Poolla, B.K., Groß, D., Dörfler, F.: Placement and implementation of grid-forming and grid-following virtual inertia and fast frequency response. *IEEE Trans. Power Syst.* 34(4), 3035–3046 (2019)
- Johnson, A.: Grid code frequency response working group system inertia. <https://www.nationalgrid.com/sites/default/files/documents/16890-Meeting-8-Inertia-presentation.pdf>. Accessed August 2021
- Tayyebi, A., Grob, D., Anta, A., Kupzog, F., Dorfler, F.: Frequency stability of synchronous machines and grid-forming power converters. *IEEE J. Emerg. Sel. Top. Power Electron.* 8(2), 1004–1018 (2020)
- Yoo, Y., Jung, S., Jang, G.: Dynamic inertia response support by energy storage system with renewable energy integration substation. *J. Mod. Power Syst. Clean Energy* 8(2), 260–266 (2020)
- Tarraso, A., Lai, N.B., Verdugo, C., Candela, J.I., Rodriguez, P.: Design of controller for virtual synchronous power plant. *IEEE Trans. Ind. Appl.* 57(4), 4033–4041 (2021)
- Task Force of the North American Electric Reliability Corp. (NERC): White paper on fast frequency response concepts and bulk power system reliability needs. <https://www.nrel.gov/grid/ieee-standard-1547/bulk-power-reliability-needs.html>. Accessed August 2021
- Fernández-Muñoz, D., Pérez-Díaz, J.I., Guisández, I., Chazarra, M., Fernández-Espina, Á.: Fast frequency control ancillary services: An international review. *Renew. Sustain. Energy Rev.* 120, 109662 (2020)
- Su, L., Qin, X., Zhang, S., Zhang, Y., Jiang, Y., Han, Y.: Fast frequency response of inverter-based resources and its impact on system frequency characteristics. *Glob. Energy Interconnect.* 3(5), 475–485 (2020)
- Badesa, L., Strbac, G., Magill, M., Stojkowska, B.: Ancillary services in Great Britain during the COVID-19 lockdown: A glimpse of the carbon-free future. *Appl. Energy* 285, 116500 (2021)
- Zhang, R., Hredzak, B.: Distributed dynamic clustering algorithm for formation of heterogeneous virtual power plants based on power requirements. *IEEE Trans. Smart Grid* 12(1), 192–204 (2021)
- Ullah, Z., Mokryani, G., Campean, F., Hu, Y.F.: Comprehensive review of VPPs planning, operation and scheduling considering the uncertainties related to renewable energy sources. *IET Energy Syst. Integr.* 1(3), 147–157 (2019)
- Knap, V., Chaudhary, S.K., Stroe, D.I., Swierczynski, M., Craciun, B.I., Teodorescu, R.: Sizing of an energy storage system for grid inertial response and primary frequency reserve. *IEEE Trans. Power Syst.* 31(5), 3447–3456 (2016)
- Niesse, A., Beer, S., Bremer, J., Hinrichs, C., Lünsdorf, O., Sonnenschein, M.: Conjoint dynamic aggregation and scheduling methods for dynamic virtual power plants. In: 2014 Federated Conference on Computer Science and Information Systems, pp. 1505–1514, IEEE, Piscataway (2014)
- Marinescu, B., Gomis-Bellmunt, O., Dörfler, F., Schulte, H., Sigrist, L.: Dynamic virtual power plant: A new concept for grid integration of renewable energy sources (2021)
- Hu, Q., Han, R., Quan, X., et al.: Grid-forming inverter enabled virtual power plants with inertia support capability. *IEEE Trans. Smart Grid* (2022)
- Sonnenschein, M., Lünsdorf, O., Bremer, J., Tröschel, M.: Decentralized control of units in smart grids for the support of renewable energy supply. *Environ. Impact Assess. Rev.* 52, 40–52 (2015)
- Adefarati, T., Bansal, R.C.: Integration of renewable distributed generators into the distribution system: a review. *IET Renew. Power Gener.* 10(7), 873–884 (2016)
- Paital, S.R., Ray, P.K., Mohanty, A.: Comprehensive review on enhancement of stability in multimachine power system with conventional and distributed generations. *IET Renew. Power Gener.* 12(16), 1854–1863 (2018)
- Mahesh, M., Bhaskar, D.V., Reddy, T.N., Sanjeevikumar, P., Holm-Nielsen, J.B.: Evaluation of ancillary services in distribution grid using large-scale battery energy storage systems. *IET Renew. Power Gener.* 14(19), 4216–4222 (2020)
- Ghasemi, H., Melki, J.: Investigation of frequency containment reserves with inertial response and batteries. Bachelor's Thesis, KTH Royal Institute of Technology, Stockholm (2019)
- Kumar, G.V.B., Palanisamy, K.: A review of energy storage participation for ancillary services in a microgrid environment. *Invent.* 5(4), 63 (2020)
- Rebours, Y.G., Kirschen, D.S., Trotignon, M., Rossignol, S.: A survey of frequency and voltage control ancillary services - Part I: Technical features. *IEEE Trans. Power Syst.* 22(1), 350–357 (2007)
- International Renewable Energy Agency (IRENA 2019): Innovation landscape brief: Innovative ancillary services. https://www.irena.org/-/media/Files/IRENA/Agency/Publication/2019/Feb/IRENA_Innovative_ancillary_services_2019.pdf?la=en&hash=F3D83E86922DEED7A A3DE3091F3E49460C9EC1A0. Accessed August 2021
- Oureilidis, K., Malamaki, K.-N., Gallos, K., et al.: Ancillary services market design in distribution networks: Review and identification of barriers. *Energies* 13(4), 917 (2020)
- Australian Energy Market Operator (AEMO): Guide to ancillary services in the National Electricity Market. https://aemo.com.au/-/media/files/electricity/nem/security_and_reliability/ancillary_services/guide-to-ancillary-services-in-the-national-electricity-market.pdf. Accessed August 2021
- Peralta, J., Cáceres, N., Saad, H., Mahseredjian, J.: Inertial and primary frequency control for MMC-based MTDC systems. In: 2018 International Conference on Power System Technology, POWERCON 2018 - Proceedings, pp. 2852–2859. IEEE, Piscataway (2019)
- Adeuyi, O.D., Cheah-Mane, M., Liang, J., Jenkins, N.: Fast frequency response from offshore multiterminal VSC-HVDC schemes. *IEEE Trans. Power Deliv.* 32(6), 2442–2452 (2017)
- Kumar, A., Meena, N.K., Singh, A.R., et al.: Strategic integration of battery energy storage systems with the provision of distributed ancillary services in active distribution systems. *Appl. Energy* 253, 113503 (2019)
- ELIA: Public consultation on the review of the black start ancillary service. <https://www.elia.be/en/public-consultation/20181005-review-of-the-black-start-ancillary-service>. Accessed August 2021
- Demoulias, C.S., Malamaki, K.-N.D., Gkavanoudis, S., et al.: Ancillary services offered by distributed renewable energy sources at the distribution grid level: An attempt at proper definition and quantification. *Appl. Sci.* 10(20), 7106 (2020)
- Fingrid: Frequency containment reserves. https://www.fingrid.fi/en/electricity-market/reserves_and_balancing/frequency-containment-reserves/. Accessed August 2021
- Bevrani, H., Raisch, J.: On virtual inertia application in power grid frequency control. *Energy Procedia* 141, 681–688 (2017)
- Eriksson, R., Modig, N., Elkington, K.: Synthetic inertia versus fast frequency response: A definition. *IET Renew. Power Gener.* 12(5), 507–514 (2018)
- Terzija, V.V.: Adaptive underfrequency load shedding based on the magnitude of the disturbance estimation. *IEEE Trans. Power Syst.* 21(3), 1260–1266 (2006)
- Garcia-Rosa, P.B., D'Arco, S., Suul, J.A.: Placement of virtual inertia from HVDC terminals based on a frequency deviation index. In: 2021 IEEE Madrid PowerTech, pp. 1–7. IEEE, Piscataway (2021)
- Pota, H.R.: MIMO systems - Transfer function to state-space. *IEEE Trans. Educ.* 39(1), 97–99 (1996)
- Li, B., Zhou, L.: Power decoupling method based on the diagonal compensating matrix for VSG-controlled parallel inverters in the microgrid. *Energies* 10(12), 2159 (2017)
- Saxena, S., Hote, Y.V.: Load frequency control in power systems via internal model control scheme and model-order reduction. *IEEE Trans. Power Syst.* 28(3), 2749–2757 (2013)
- Sonker, B., Kumar, D., Samuel, P.: Dual loop IMC structure for load frequency control issue of multi-area multi-sources power systems. *Int. J. Electr. Power Energy Syst.* 112, 476–494 (2019)
- Tan, W.: Unified tuning of PID load frequency controller for power systems via IMC. *IEEE Trans. Power Syst.* 25(1), 341–350 (2010)

42. Saxena, S., Hote, Y.V.: Advances in internal model control technique: A review and future prospects. *IETE Tech. Rev.* 29(6), 461–472 (2012)
43. Chaves, E.N., Coelho, E.A.A., Carvalho, H.T.M., Freitas, L.C.G., Joao, B. V., Freitas, L.C.: Internal model control design applied to single-phase grid-connected inverters. In: 2015 IEEE 13th Brazilian Power Electronics Conference and 1st Southern Power Electronics Conference, COBEP/SPEC 2016. IEEE, Piscataway (2015)
44. Mohapatra, S.R., Sekhar, P., Agarwal, V., Patwardhan, S.C.: Experimental evaluation of internal model control for 3 ϕ grid-tied solar PV inverter. In: 2020 International Conference on Power Electronics and IoT Applications in Renewable Energy and its Control, PARC 2020, pp. 432–436. IEEE, Piscataway (2020)
45. Arya, P.P., Chakrabarty, S.: A robust internal model-based fractional-order controller for fractional-order plus time delay processes. *IEEE Control Syst. Lett.* 4(4), 862–867 (2020)
46. Chow, J.: Power system toolbox webpage. <https://www.ecse.rpi.edu/~chowj/>. Accessed September 2015
47. Sturk, C., Vanfretti, L., Milano, F., Sandberg, H.: Structured model reduction of power systems. In: Proceedings of the American Control Conference, pp. 2276–2282. IEEE, Piscataway (2012)
48. Kundur, P.: *Power System Stability and Control*. McGraw-Hill, Inc., New York (1994)
49. NEPLAN smarter tools: Turbine-governor models, standard dynamic turbine-governor systems in NEPLAN power system analysis tool. https://www.neplan.ch/wp-content/uploads/2015/08/Nep_TURBINES_GOV.pdf. Accessed April 2021
50. Soonee, S.K., Baba, K.V.S., Barpanda, S.S., et al.: Ancillary services in India-evolution, implementation and benefits. In: National Power System Conference. IEEE, Piscataway (2016)
51. Zhu, Y., Liu, C., Sun, K., Shi, D., Wang, Z.: Optimization of battery energy storage to improve power system oscillation damping. *IEEE Trans. Sustain. Energy* 10(3), 1015–1024 (2019)
52. Liu, L., Li, W., Ba, Y., Shen, J., Jin, C., Wen, K.: An analytical model for frequency Nadir prediction following a major disturbance. *IEEE Trans. Power Syst.* 35(4), 2527–2536 (2020)
53. Wen, Y., Li, W., Huang, G., Liu, X.: Frequency dynamics constrained unit commitment with battery energy storage. *IEEE Trans. Power Syst.* 31(6), 5115–5125 (2016)
54. Zografos, D., Ghandhari, M.: Estimation of power system inertia. In: IEEE Power and Energy Society General Meeting. IEEE Computer Society, Los Alamitos (2016)
55. Akram, U., Mithulananthan, N., Shah, R.: Improving synthetic inertial response of supercapacitor using supplementary control signal. In: 2019 9th International Conference on Power and Energy Systems, ICPES 2019. IEEE, Piscataway (2019)

How to cite this article: Kumar, L., Ahmed, S., Naidoo, R., Bansal, R.C.: Decentralized reinforce-control of renewable dynamic virtual power plant enabling it to offer ancillary services: An attempt towards net-zero targets. *IET Renew. Power Gener.* 17, 2512–2530 (2023). <https://doi.org/10.1049/rpg2.12545>

TABLE A1 Parameters of TGs

Thermal (Figure 8)			Hydro (Figure 9)		
ω_f	Angular speed set point	1	ω_f	Angular speed set point	1
r	Droop	0.04	r_p	Permanent droop	0.04
T_s	Servo time constant	0.1	r_t	Transient droop	0.38
T_c	Governor time constant	0.5	T_s	Servo time constant	0.07
T_3	Transient gain time constant	0	K_s	Servo gain	3.33
T_4	HP section time constant	1.25	T_g	Governor time constant	0.2
T_5	Reheater time constant	5	T_r	Reset time constant	0.2
			T_w	Water starting time	2.67

APPENDIX

Putting the TGs' TFs, $G_{r,m}^1$ and $G_{b,m}^1$ from Equations (43) and (44), respectively, in Equation (56), $e_{hydro}(s)$ can be obtained as;

$$e_{hydro}(s) = \frac{-G_{b,m}^1(s)}{-G_{r,m}^1(s)} = \frac{\left(\frac{K_s(T_r s + 1)}{T_r T_r s^3 + (T_r + T_r)s^2 + T_r(r_p + r_t)s + K_s r_p} \right) \cdot \left(\frac{1}{1 + T_g s} \right) \cdot \left(\frac{1 - s T_w}{1 + s \frac{T_w}{2}} \right)}{\frac{1}{r} \cdot \left(\frac{1}{1 + iT_s} \right) \cdot \left(\frac{1 + iT_3}{1 + iT_c} \right) \cdot \left(\frac{1 + iT_4}{1 + iT_5} \right)} \quad (A1)$$

By putting the parameters from Table A1, the above Equation (A1) end up with the RHS in Equation (56). T_{BESS} and T_{SC} in Equation (52) can be obtained from Equation (57) and Equation (58), respectively, as follows;

$$T_{BESS}(s) = e_{BESS}(s) \cdot T_{des}(s) = \frac{-437.5s(s + 10.86)(s + 2.98)(s + 0.95)(s + 0.29)}{(s + 13.67)(s + 5.49)(s + 1)(s + 0.8)(s + 0.75)(s + 10)(s + 2)(s + 0.2)} \quad (A2)$$

$$T_{SC}(s) = e_{SC}(s) \cdot T_{des}(s) = \frac{-125s(s + 14.3)(s + 5.9)(s + 0.19)(s^2 + 1.76s + 0.8)}{(s + 13.67)(s + 5.49)(s + 1)(s + 0.13)(s + 0.75)(s + 10)(s + 2)(s + 0.2)} \quad (A3)$$